Soils and Rocks
An International Journal of Geotechnical and Geoenvironmental Engineering
www.soilsandrocks.com
ISSN 1980-9743
ISSN-e 2675-5475

Dynamic driving formulas and static loadings in the light of wave equation solutions

Faiçal Massad[1#]

Article

Keywords
Dynamic formulas
Driven piles
Bearing capacity
Static and dynamic displacements
Elastic rebounds

Abstract

The advances in pile monitoring have motivated attempts to support dynamic formulas to estimate pile bearing capacity. Based on numerical analysis of the wave equation and the results of dynamic loading tests in three piles the paper deals with the investigation of the soundness of some of the most used in Brazil, namely, the so called Chellis-Velloso Formula, the Energy Approach Equation and Uto's Formula. The former gained strength through a misinterpretation of Casagrande (1942) statement that the elastic compression of a pile during driving is a measure of the dynamic force with which the soil is tested, and not of its static resistance. Therefore, the elastic compression and rebound, measured during driving, are generally smaller than the corresponding static values. The second is based on an elasto-plastic load-displacement relationship without physical meaning, besides the fact that the effective energy in driving a pile is related to the work of dynamic forces and has nothing to do with the static resistances. The third was derived from a simplified solution of the wave equation, assuming among other hypothesis that there is no friction along pile shaft. The paper shows the ineffectiveness of attempts to universally validate these formulas with dynamic pile monitoring and the implications in the simulation of static loadings.

1. Introduction

Dynamic formulas have the appeal of their simplicity, especially those that depend on the set (s), the elastic rebound (K) and the efficiency (η) of the driving system. The trend today is to take advantage of the dynamic monitoring of a certain number of piles and obtain parameters such as η to be used in other piles of the work along with direct measurements of s and K, say, with pencil and paper.

However, some of the most used dynamic formulas in Brazil, namely the Chellis-Velloso Formula, the Energy Approach Equation, and the Uto's Formula have required adjustments considering the geometry and kind of piles, the types of soils, among other factors. The question that arises refers to the general validity of these formulas.

Furthermore, in this context the simulation of static loadings through dynamic tests with increasing energy is discussed.

2. The Chellis-Velloso formula

The well-known formula of Chellis (1951) modified by Velloso (1987) is based on Hooke's law and uses measurements of elastic rebound to estimate static resistance, as shown in Equations 1 and 2.

$$R = \frac{C_2 \cdot E \cdot S}{\alpha \cdot L} = \frac{(K - C_3) \cdot K_r}{\alpha} \quad (1)$$

$$K_r = \frac{E \cdot S}{L} \quad (2)$$

In these equations $R=RMX$ is the static mobilized resistance; K_r, the pile stiffness; C_2, the pile elastic shortening or pile compression; E, the dynamic Young's modulus; S, the area of the pile cross section; L, its length; K, the elastic rebound; C_3, the toe "quake", usually taken equal to 2.5mm; and α, a factor dependent on the distribution of lateral friction and tip load, given by:

$$\alpha \cong \beta + \lambda \cdot (1 - \beta) \quad (3)$$

where λ is the coefficient of Leonards & Lovell (1979) and β is the relationship between tip load and total load. Velloso (1987) suggested using α =0.7, an average value.

#Corresponding author. E-mail address: faical.massad@usp.br
[1]Universidade de São Paulo, Escola Politécnica, São Paulo, SP, Brasil.

Submitted on January 4, 2021; Final Acceptance on April 21, 2021; Discussion open until August 31, 2021.
https://doi.org/10.28927/SR.2021.061921

3. The energy approach equation

The Energy Approach Equation, as presented by Paikowsky & Chernauskas (1992), takes the form of Equation 4.

$$R_u = RMX = \frac{2.\kappa.EMX}{s + DMX} \quad (4)$$

These authors assumed an elasto-plastic relation between resistance and displacement, as shown in Figure 1. The maximum energy delivered to the pile (*EMX*) was equated to the work done by the resistance (R_u *or RMX*) offered by the soil to the penetration of the pile [*RMX.(s+DMX)/2*], where *DMX=s+K*. Based on a case study, Paikowsky & Chernauskas (1992) proposed a reduction parameter κ=0.8, arguing that part of the applied energy *EMX* is dissipated in the mobilization of viscous or dynamic resistances.

Aoki (1997) interpreted the driving process in the light of the Hamilton's Principle of energy conservation and came up with a similar expression, using the ζ symbol instead of *2κ*. The parameter ζ would depend on the magnitude and nature of the reaction forces (conservative or non-conservative) and could vary between 1 (permanent displacement predominates) and 2 (elastic displacement predominates).

4. The Utos's formula

Uto et al. (1985) presented a simple formula based on the solution of one-dimensional wave equation, admitting as the boundary condition the displacement-time curves for the top and the tip of the pile. Several simplifying hypotheses were assumed, among which the following stand out: a) lateral friction and viscous resistance (damping) at the tip of the pile were neglected during driving; and b) the set (*s*) was taken equal to the toe quake (C_3). They came to the following equations:

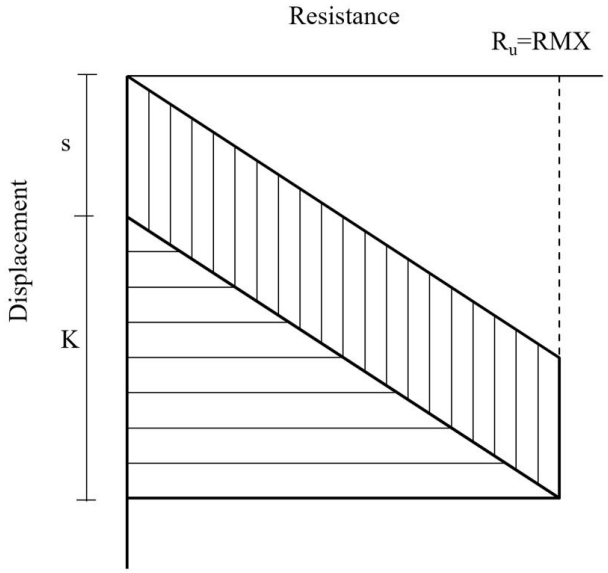

Figure 1. Resistance vs displacement.

$$R_d^{tip} = \frac{K_D \cdot E \cdot S}{e_o.L} = \frac{K_D.K_r}{e_o} \quad (5)$$

$$e_o = \left(\xi.\frac{W_H}{W_P}\right)^{\frac{1}{3}} \quad (6)$$

where R_d^{tip} is the dynamic resistance mobilized at the pile tip; e_o, a wavelength correction factor, is a function of both, (a) the relationship between the weights of the hammer (W_H) and the pile (W_P), and (b) the pile type, through the parameter ξ, that assumes a figure of 1.5 for steel piles and 2.0 for concrete piles.

5. Differences in C_2 and K static and dynamic

5.1 Theoretical background

For the pile element in Figure 2a, the equation of the balance of the acting forces during driving can be written as follows (see attached list of symbols):

$$F = \pi.D.f.dx + (F + dF) + \rho.S.dx.\frac{d^2u}{dt^2} \quad (7)$$

According to Smith (1960), the shaft friction (*f*) is given by:

$$f = k.u.\left(1 + J.\frac{du}{dt}\right) = f^{est}.\left(1 + J.\frac{du}{dt}\right) \quad (8)$$

valid for *u* smaller than the quake. If not, *k.u* is equal to the maximum shaft friction (f_{max}^{est}).

Equation 7 may be rewritten as:

$$\frac{dF}{dx} = -\pi.D.f - \rho.S.\frac{d^2u}{dt^2} \ \ with \ \ \rho.S = \frac{E,S}{c^2} \quad (9)$$

Note that:

$$\pi.D.f.dx = R_m = R_d + R_e \quad (10)$$

where R_e, R_d and R_m are respectively the static, dynamic, and total resistances in the element. By Hooke's Law it follows:

$$\varepsilon = -\frac{du}{dx} = \frac{F}{E \cdot S} \quad (11)$$

This equation shows that it is the dynamic force *F* that generates the elastic shortenings (*du*) in the element and not the static force R_e, confirming the above-mentioned statement of Casagrande (1942).

By deriving both members from Equation 11 the term *dF/dx* is obtained, which, replaced in Equation 9, results in the Wave Equation:

$$\frac{d^2u}{dx^2} = \frac{\pi \cdot D \cdot f}{E \cdot S} + \frac{\rho}{E} \cdot \frac{d^2u}{dt^2} \quad (12)$$

At time *t*, *F* varies as follows along depth (*x*):

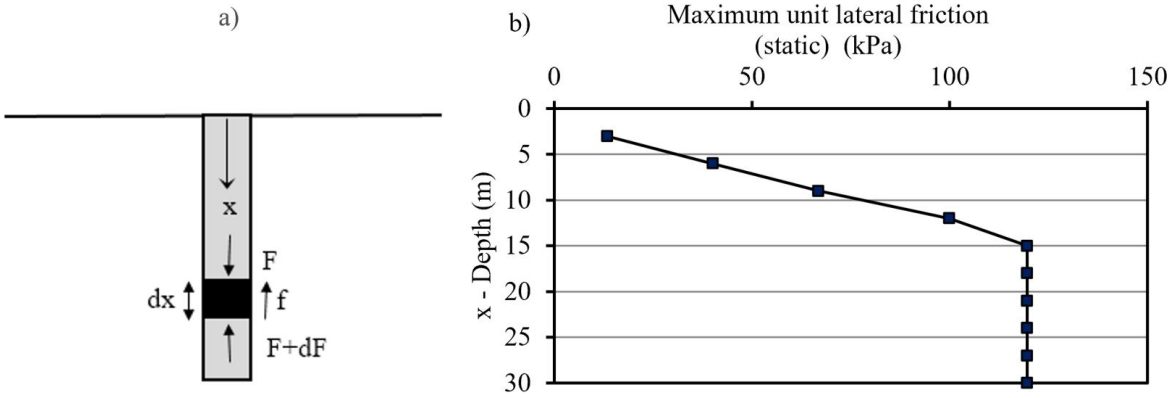

Figure 2. (a) Forces and stresses in pile element of height dx; (b) Maximum unit lateral friction (static) vs depth.

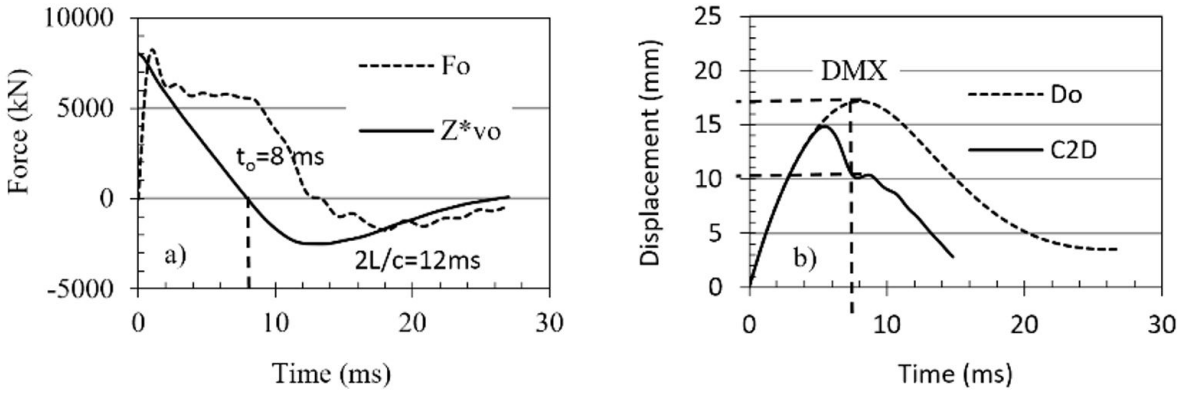

Figure 3. Forces (a) and displacements (b) vs time, with v_o=4.33 m/s at t=0.

$$F(x) = F_o - \sum_0^x R_m - \frac{E.S}{c^2} \cdot \int_0^x \frac{d^2u}{dt^2} \cdot dx \quad (13)$$

where F_o stands for $F(x)$ at pile top (x=0).

5.2 Numerical wave equation solutions for simple cases

Consider the solution of the wave equation presented in Figure 3a obtained through the methodology of Smith (1960) applied to a steel pipe pile (see Table 1), excited at the top by a speed v_o=4.33 m/s at time t=0, due to the blow of a hammer. It was assumed that static maximum unit lateral frictions (Figure 2b) are known a priori just like the toe static resistance (R_p), the shaft (q_s) and tip (q_t) quakes, and "Smith dampings" of friction (J_s) and tip (J_t), indicated in Table 2. Under these conditions, the maximum static lateral (A_{lr}) and tip (Q_{pr}= R_p. S_p) loads are 8081 kN and 1225 kN, respectively, adding up 9306 kN.

From Figure 3a one may conclude that for t=t_o=8 ms the speed at the top (v_o) is zero and therefore the displacement at the top reaches its maximum value, *DMX* in Figure 3b. This figure also displays the calculated C_{2D} by the difference of the top and tip pile displacements at each time. For the same time t=8 ms, Figure 4 shows the distribution along the shaft of the maximum static resistance and of the dynamic (F) axial force. From its analysis, it can be concluded that (see the list of symbols attached):

a) the forces F for t=8 ms were lower than the maximum static resistances (Figure 4), with C_{2D}=10.1 mm (Figure 3b) which is smaller than the corresponding static value, given by:

$$C_{2E} = \frac{\lambda * A_{lr} + Q_{pr}}{K_r} = \frac{0.6 * 8081 + 1225}{316} \cong 19.2\,mm \quad (14)$$

and K_D=C_{2D}+q_t≈11.8 mm against K_E= C_{2E}+C_3 ≈20.9 mm. As *DMX*=17.1 mm (Figure 3b), it follows that s=*DMX*-K_D=5.3mm; the values of λ and K_r are given in Tables 1 and 2; and

b) these differences between static and dynamic values (Figure 4) result from Equation 13: the total resistances (R_m) interact with the inertial forces, due to acceleration, which acts either up or down, as illustrated in Figure 5.

The same Pile E-1 was also submitted to a simulation of the dynamic loading test with increasing energy, as proposed by Aoki (1989). The speed at the top due to the impact of the hammer was varied between 1.08 and 6.49 m/s, which implied in *EMX* increasing from 6 to 228 kN.m, as shown in Table 3

Table 1. Characteristic of pile excited with v_o=4.33 m/s at time t=0.

Pile	D_e (cm)	D_i (cm)	S (cm²)	S_p (cm²)	L (m)	E (GPa)	K_r (kN/mm)	c (m/s)
E-1	91.4	88.2	451.4	6561	30	210	316	5125

Legend: see attached list of symbols.

Table 2. Assumed parameters for Pile E-01.

Pile	λ	R_p (kPa)	q_s (mm)	q_t=C_3 (mm)	J_s (s/m)	J_t (s/m)
E-1	0.6	1867	5.73	1.76	0.12	0.18

Legend: see attached list of symbols.

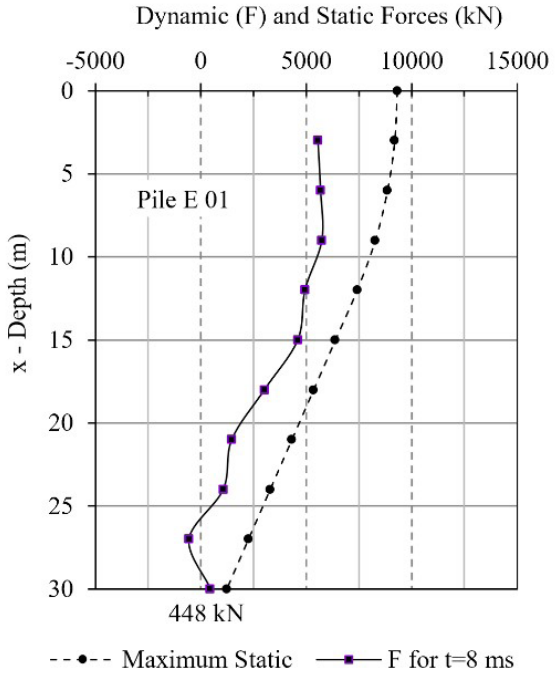

Figure 4. Axial Forces vs depth (v_o=4.33 m/s at t=0).

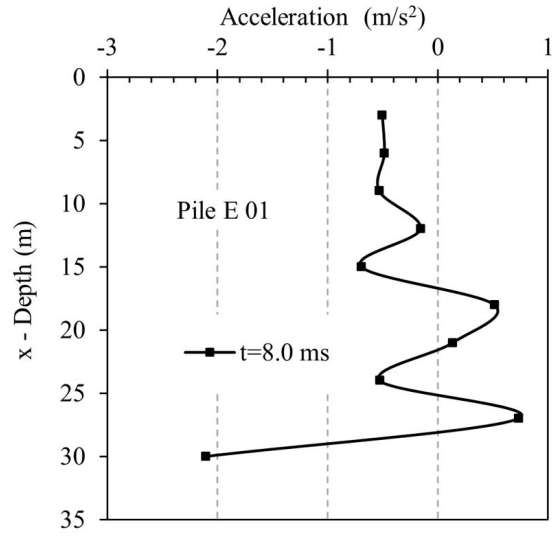

Figure 5. Acceleration vs depth (v_o=4.33 m/s at t=0).

with other data of this simulation; note that the set varies with time (s_{to}<s_{tf}). The results in Table 4 confirms that the dynamic values of elastic compression (C_{2D}) and rebound (K_D) are lower than the corresponding static values (C_{2E} and K_E).

5.3 Evaluation of Chellis-Velloso formula

The differences between static and dynamic values of C2 lead to the first conclusion about the Chellis-Velloso Formula, Equations 1 to 3. With the values of K_r=316 kN/mm (Table 1), λ=0.60 (Table 2) and β=1225/9306=13.2% it follows for blow 5 of Tables 3 and 4:

$$\alpha \cong 0.132 + 0.6 \cdot (1 - 0.132) = 0.652 \quad (15)$$

$$R = \frac{10.1 * 316}{0.652} = 4895\,kN \quad (16)$$

much smaller than:

$$R = \frac{19,2 * 316}{0.652} = 9306\,kN \quad (17)$$

confirming the note of Velloso & Lopes (2002) that Equation 1 refers to static calculation. And these authors added that this formula may be valid for short piles, with lengths of the order of the wavelength and so the whole pile is compressed, which does not occur on long piles.

6. Force or resistance vs displacement. Evaluation of the energy approach equation

Figure 6 shows the progress of the mobilized static resistance (R_e) along the depth (x) and the time (t). For t=8 ms the static resistances in the elements (R_e) already reach the maximum available values.

Figure 7 reveals that the total static (R_{eT}) and the total dynamic+static resistances (R_{mT}=R_{eT}+R_{dT}) reach maximum values at a time t≈7 ms, therefore close to 8 ms, at which time the maximum displacement (DMX) occurs, as seen above (Figure 3b). It is also interesting to note that as time proceeds, the portions of the dynamic resistances vanish, as the pile is no more in movement.

The dynamic displacement (D_m) progresses along the depth (x) and time t (from 2 to 8 ms) as shown in Figure 8.

Table 3. Data on simulated dynamic loading tests with increasing energy - Pile E-1.

Blow #	v_o (t=0) (m/s)	EMX (kN.m)	t_o (ms)	RMX (kN)	DMX (mm)	s_{to} (mm)	s_f (mm)
1	1.08	6	7.6	4168	4.1	0.0	0.0
2	1.50	12	7.6	5451	5.8	0.4	0.4
3	2.16	25	7.6	7015	8.4	1.5	1.6
4	3.05	50	7.6	8643	12.0	3.1	3.1
5	4.33	101	8.0	9306	17.1	5.3	5.9
6	6.49	228	8.4	9306	26.4	10.6	14.8

Legend: see attached list of symbols.

Table 4. Other results of increasing energy loading tests - Pile E-1.

Blow #	v_o (t=0) (m/s)	C_{2D} (mm)	C_{2E} (mm)	K_D (mm)	K_E (mm)
1	1.08	2.6	8.7	4.1	10.4
2	1.50	3.6	11.0	5.4	12.8
3	2.16	5.1	13.9	6.9	15.6
4	3.05	7.1	17.2	8.9	19.0
5	4.33	10.1	19.2	11.8	20.9
6	6.49	14.0	19.2	15.8	20.9

Legend: see attached list of symbols.

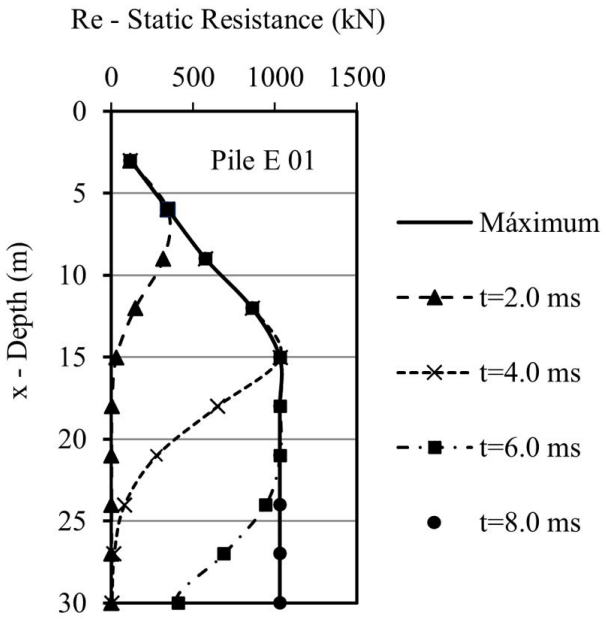

Figure 6. Static Resistances vs depth and time (v_o=4.33 m/s at t=0).

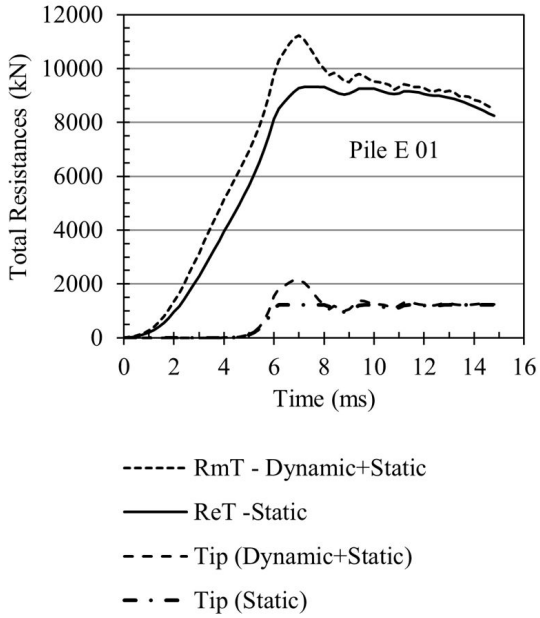

Figure 7. Total Resistances vs time (v_o=4.33 m/s at t=0).

Figure 9 shows that there is a mismatch between the mobilization of the R_{eT} and the development of displacements at the top (D_o): D_o grows faster than R_{eT}.

Moreover, the relationship between the total static resistance (R_{eT}) and the dynamic displacement at the top (D_o) (Figure 10) is not elasto-plastic, as is supposed by the Energy Approach Equation (Equation 4 and Figure 1). It is concluded, therefore, that this equation does not represent reality: it is a fiction.

Figure 11 is an extension of Figure 10, as it includes all blows of Tables 3 and 4, in addition to blow 5 (v_o=4.33 m/s at t=0). It also includes the envelop representing the curve *RMX* as a function of *DMX*. This same curve is reproduced in Figure 12, along with two others: a) the *RMX* curve as a function of *DMX* plus the sets of the previous blows, as proposed by Aoki (1989) and Niyama & Aoki (1991);

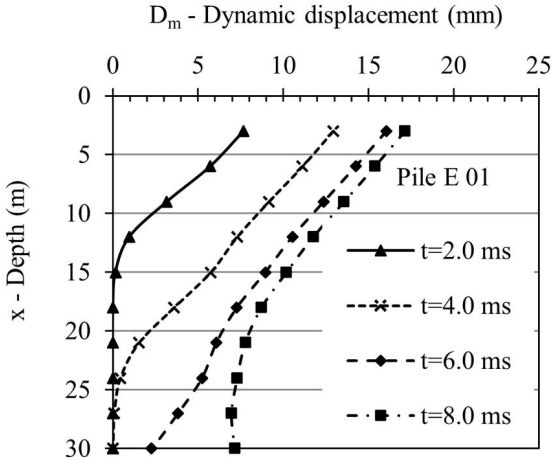

Figure 8. Dynamic Displacements vs depth and time (v_o=4.33 m/s at t=0).

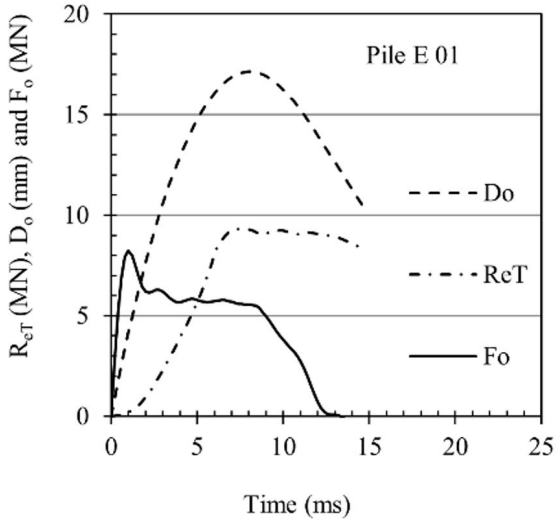

Figure 9. Force, Resistance and Displacement along time (v_o=4.33 m/s at t=0).

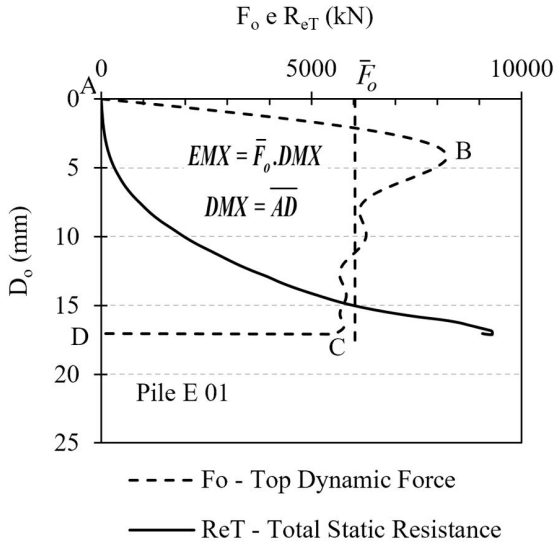

Figure 10. Force or Resistance vs. Displacement (D_o) (v_o=4.33 m/s at t=0).

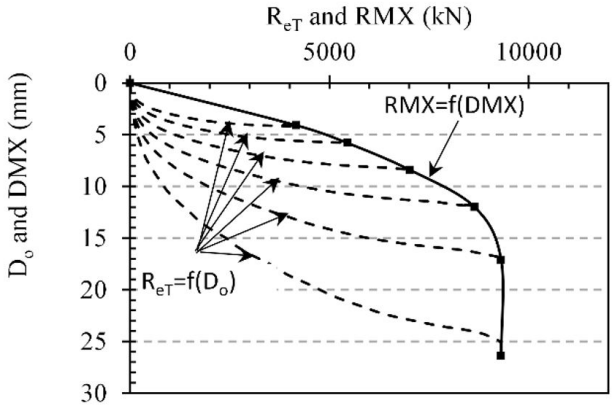

Figure 11. Resistances vs. D_o and R_{eT} (Blows of Tables 3 and 4).

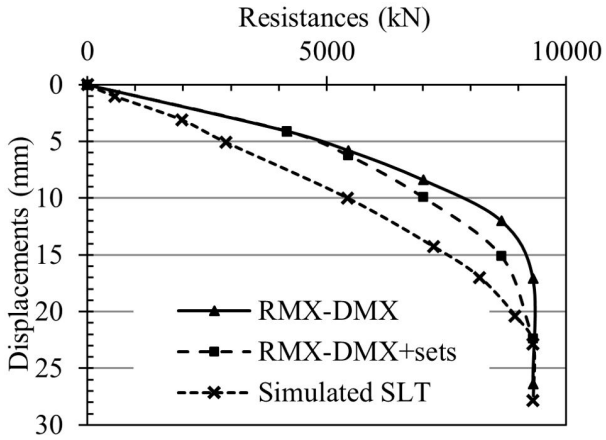

Figure 12. Resistances-Displacements curves (Blows of Tables 3 and 4).

and b) the load-displacement curve for blow 6 of Table 3 simulating the static loading test (SLT) obtained through the Method of Coyle & Reese (1966), considering the maximum resistances, quakes, and pile stiffness. It is concluded that for the analyzed pile E-1 the Aoki-Niyama curve falls short of the simulated curve.

At time t≈8 ms v_o=0 (Figure 3a), *D(t)* and *E(t)* reach the maximum values, *DMX* and *EMX*, respectively. The $F_o.v_o$ product assumes negative values between 8 and 13 ms (Figure 13a), hence the inflection in the *E(t)* curve as displayed in Figure 13-b. The value of *EMX* can be obtained as shown in Equation 18, where $\bar{F}_o$ is an average value between t=0 and t=8 ms. In fact, the third term in this equation is a result of the application of the Mean Value Theorem (Pastor et al., 1958), because in the interval 0 to 8 ms the following inequation holds: $F_o.v_o \geq 0$.

$$EMX = \int_0^{t_o} F_o v_o dt = \bar{F}_o \cdot \int_0^8 v_o dt = \bar{F}_o \left[D(8) - D(0) \right] = \bar{F}_o DMX \quad (18)$$

Another conclusion arises from the *ABCD* curve of Figure 10, which represents the variation of F_o with D_o between 0 and t=8 ms. The area bounded by this curve corresponds

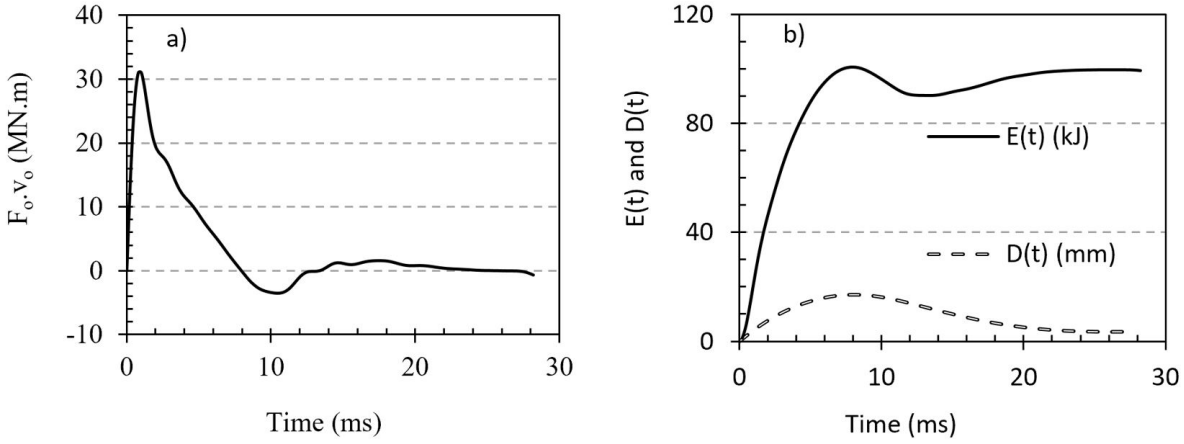

Figure 13. a) The product $F_o.v_o$ vs time and b) Energy (E) and Displacement (D) vs time.

to the *EMX* value, which has nothing to do with the work of total static resistance R_{eT}, putting again the Energy Approach Equation in question.

7. Evaluation of Uto's formula

Another conclusion refers to the application of the Uto's Formula, Equations 5 and 6. For the type of pile (E-1) the correction factor e_o (Equation 6) assumes a value of the order of 1.10, so that for blow 5 of Table 4:

$$R_d^{tip} = \frac{11.8 * 316}{1.10} \cong 3390\,kN \gg 448\,kN\ (see\ Figure 4) \quad (19)$$

It is interesting to mention the results indicated in Figure 14, related to pile E-1, blow 5 (v_o=4.33 m/s at t=0), but assuming that the maximum static lateral and tip loads are 5000 kN and 4306 kN, respectively, adding up the same total static load 9306 kN. The distribution of the shaft friction (f) along depth was supposed to be the same (λ=0.6).

Figure 14 shows that for t=8.8 ms the dynamic force F is resisted only by the tip, with R_d^{tip} =4078 kN. As K_D=15.3, the Uto's Formula gives:

$$R_d^{tip} = \frac{15.3 * 316}{1.10} \cong 4400\,kN \quad (20)$$

about 8% more. This case fulfills one of the conditions of Uto´s Formula, i.e, practically no dynamic shaft friction.

8. Evidence from three case histories

Next, results of dynamic loading tests with increasing energy on three case histories comprising pipe piles will be presented. The piles were quite different as shown in Table 5.

The subsoil in the case of Osasco (SP) consisted of 3.5 m of a landfill (SPT=4 to 5), followed by layers of soft fluvial clays up to 9.1 m (SPT=1 to 3) and residual soil (SPT=25 to 55). The water level was 3 m deep.

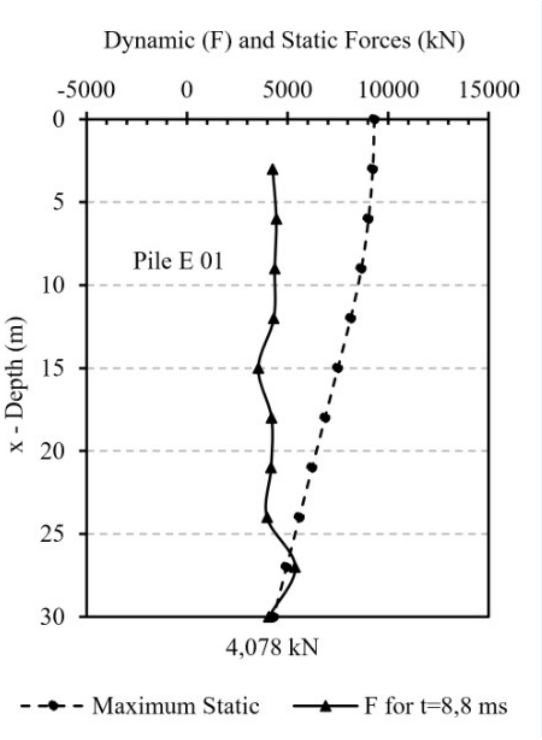

Figure 14. Axial Forces vs depth (v_o=4.33 m/s at t=0 and max. static tip load =4306 kN).

In the case of a pier of Santos (SP), below 6 m of water there was a layer of 20 m of a soft Holocene clay (SPT=1 to 5), followed by 10 m of fine clayey sand (SPT=7 to 33) and 8 m of a Pleistocene clay (SPT~7) over thick sand layer (SPT~40).

Finally, the subsoil in Cubatão (SP) consisted of sandy fill 6 m thick (SPT=1 to 10), followed by a layer of a Holocene marine clay (SPT=1 to 5) up to 24 m deep. Below there were two layers of sand (SPT=15 to 30 and 30 to 15, respectively) up to roughly 40 meters deep, followed by residual soil of gneiss. The water level was 1 m deep.

Details of the hammers and of the instruments that were used and the sequence of blows in each pile are presented in the references shown in Table 5. The collected data were analyzed through the CAPWAP software by specialized technicians, with match quality control. Static loading simulations were made for the blows of maximum energy. Some results of dynamic loading tests on these piles are presented in Table 6 and in Figures 15 to 17.

Table 5. Characteristic of the piles submitted to dynamic loading tests.

Case	*Type*	D_e (cm)	D_i (cm)	*L (m)*	L_c (m)	Reference
1. Osasco	Concrete	38.0	20.3	14.1	13.8	Murakami & Massad (2016)
2. Santos	Concrete	80.0	50.0	52.0	43.4	Valverde & Massad (2018)
3. Cubatão	Steel pipe	91.4	88.2	40.1	33.3	Valverde & Massad (2018)

Legend: see attached list of symbols.

Table 6. Dynamic loading tests results for the blows of maximum energy.

Case	*Kr (kN/mm)*	*EMX (kN.m)*	*RMX (kN)*	*DMX (mm)*	A_l (kN)	Q_p (kN)
Osasco	253	20.8	2001	12.5	1001	1000
Santos	201	133.2	8041	26.4	6225	1816
Cubatão	280	84.4	559	16.4	4647	4912

Legend: see attached list of symbols.

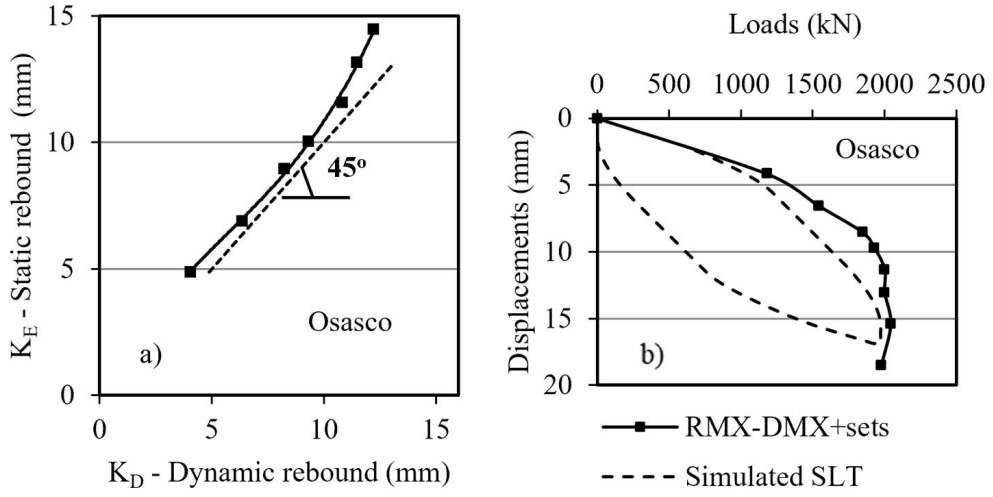

Figure 15. First case history - a) K_E vs K_D and b) Loads vs displacements.

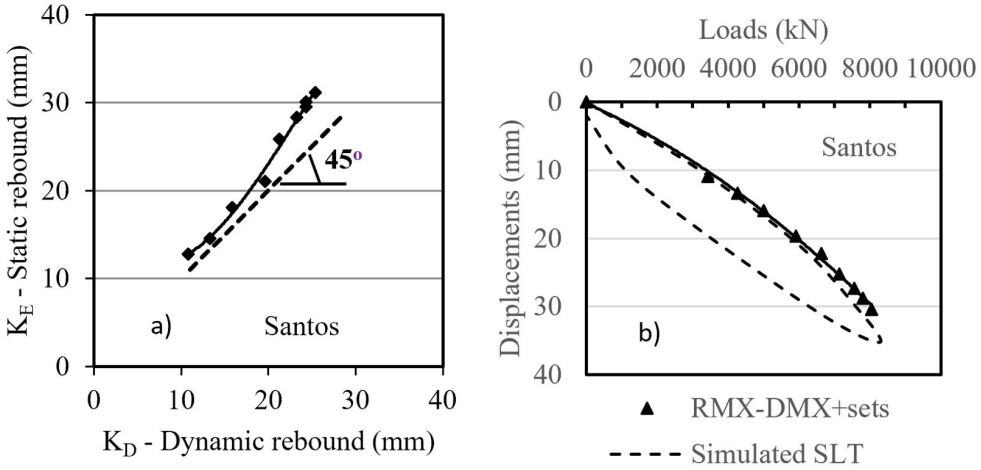

Figure 16. Second case history - a) K_E vs K_D and b) Loads vs displacements.

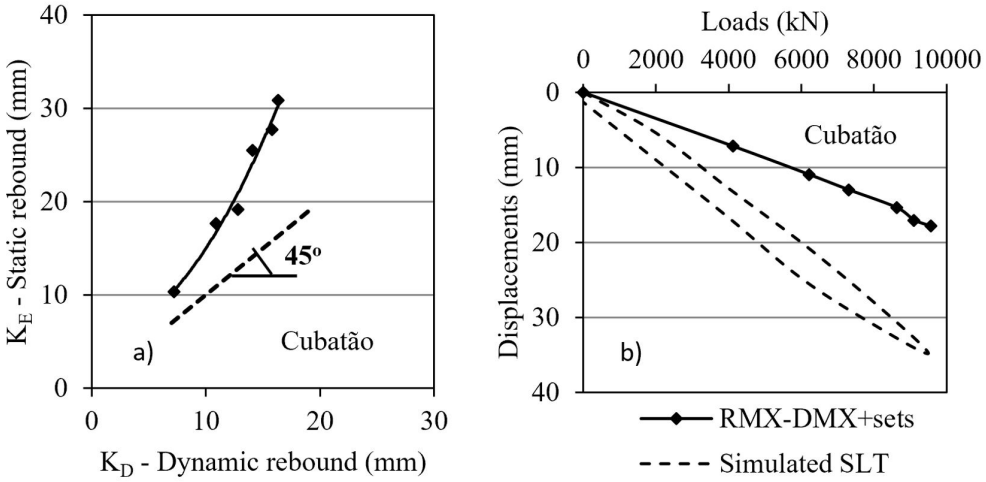

Figure 17. Third case history - a) K_E vs K_D and b) Loads vs displacements.

As can be seen, there are different behaviors in terms of: a) the rebounds K_E and K_D, on the one hand; and b) of the load-displacement curves, on the other hand. In fact:

a) the elastic rebounds (K_D), measured during pile driving, are lower than the corresponding static values (K_E), again because they are related to the dynamic forces and not to the resistance of the soil, as Casagrande intuited; and
b) the curves *RMX-DMX* plus the sets of the previous blows fall short of the simulated static curves with only 1 stroke. The pile in Santos (Figure 16) was an exception, due to higher values of the set (*s*), accumulating about 5mm up to the last stroke.

These differences depend on several factors, such as the distribution of the load in depth (friction and tip), the set values, among others. The phenomenon of pile driving is quite complex.

9. Conclusions

Elastic compression and rebound measured during pile driving may be lower than the corresponding static values because they are related to the dynamic forces and not to the static resistance of the soil, as Casagrande intuited.

This fact explains why the curve *RMX-DMX* plus the sets of the previous blows can fall short of the simulated static curve with one single stroke. Moreover, it conceptually invalidates the use of the Chellis-Velloso Formula to estimate the bearing capacity of a pile.

This last conclusion extends to the Energy Approach Equation based on an elasto-plastic relationship without physical meaning; furthermore, it wrongly relates the transferred energy (*EMX*) to the work of the soil resistances instead of the involved dynamic forces.

The Uto's Formula has restricted use in view of the adopted hypotheses, allowing its application to determine the dynamic force at the tip in cases where lateral friction is exceedingly small.

This makes conceptually unsuccessful attempts to universally validate these formulas. But nothing prevents their use in engineering practice as empirical correlations with correction factors, supported by the dynamic monitoring of some piles of a given work and place.

Acknowledgements

The author thanks the support received from the Polytechnic School of São Paulo University.

Declaration of interest

The author declares absence of conflicting interests.

Author's contributions

Faiçal Massad: conceptualization, methodology, validation, writing, and editing.

References

Aoki, N. (1997). *Determinação da capacidade de carga última de estaca cravada em ensaio de carregamento dinâmico de energia crescente* [Unpublished doctoral dissertation]. Engineering School of São Carlos, University of Sao Paulo. In Portuguese.

Aoki, N. (1989). A new dynamic load test concept. In *Proceedings of the XII International Conference on Soil Mechanics and Foundation Engineering* (pp. 1-4, Discussion section 14), Rio de Janeiro. ISSMGE.

Casagrande, A. (1942). Discussions on the progress report of the Committee on the Bearing Value of Pile Foundations. *Proceedings of the ASCE*, 68(2), 324-331.

Chellis, R.D. (1951). *Pile foundations.* New York: McGraw-Hill Company.

Coyle, H.M., & Reese, L.C. (1966). Load transfer for axially loaded piles in clay. *Journal of the Soil Mechanics and Foundations Division*, 92(2), 1-26. http://dx.doi.org/10.1061/JSFEAQ.0000850.

Leonards, G.A., & Lovell, D. (1979). Interpretation of load tests on high-capacity driven piles. In R. Lundgren (Ed.), *Behavior of deep foundations* (pp. 388-415). Philadelphia: ASTM International.

Murakami, D.K., & Massad, F. (2016). Determinação do quake de estacas pré-moldadas de concreto através de provas de carga estática e ensaios de carregamento dinâmico. *Geotecnia*, 137, 79-98. http://dx.doi.org/10.24849/j.geot.2016.137.05.

Niyama, S., & Aoki, N. (1991). Correlations between static and dynamic load tests in the experimental field of EPUSP. In *Proceedings of the 2nd Seminar on Special Foundations and Geotechnical Engineering* (Vol. 1, pp. 285-293). São Paulo: ABEF.

Paikowsky, S.G., & Chernauskas, L.R. (1992). Energy Approach for capacity evaluation of driven piles. In *Proceedings of the 4th International Conference on the Application of Stress-Wave Theory to Piles* (pp. 21-24). Philadelphia: ASTM International.

Pastor, J.R., Calleja, P., & Trejo, C.A. (1958). *Análisis matemático* (Vol. 1). Buenos Aires Editorial Kapelusz. In Spanish.

Smith, E.A.L. (1960). Pile driving analysis by the wave equation. *Journal of the Soil Mechanics and Foundations Division*, 86(4), 35-61. http://dx.doi.org/10.1061/JSFEAQ.0000281.

Uto, K., Fuyuki, M., & Sakurai, M. (1985). An equation for the dynamic bearing capacity of a pile based on wave theory. In *Proceedings of the International Symposium on Penetrability and Drivability of Piles* (pp. 201-204). Tokyo: Japanese Geotechnical Society.

Valverde, R., & Massad, F. (2018). Maximum envelope of lateral resistance through dynamic increasing energy test in piles. *Soils and Rocks*, 41(1), 75-88. http://dx.doi.org/10.28927/SR.411075.

Velloso, D.A., & Lopes, F.R. (2002). *Fundações profundas* (Vol. 2). Rio de Janeiro: COPPE-UFRJ.

Velloso, P.P.C. (1987). *Fundações: aspectos geotécnicos* (5. ed., Vol. 2-3). Rio de Janeiro: Departamento de Engenharia Civil, PUC.

List of symbols

A_l	Static lateral load
A_{lr}	Maximum static lateral load
c	Wave velocity
C_2	Pile elastic shortening
C_{2D}	Dynamic Pile elastic shortening
C_{2E}	Static Pile elastic shortening
C_3	Toe quake
$D_i;D_e$	Inside and outside pile diameters
D_m	Dynamic displacement
D_o	Value of D_m at pile top (x=0)
DMX	Maximum value of D_m
E Pile	Young's Modulus
EMX	Maximum transferred energy
e_o	Uto's wavelength correction factor (see Equation 6)
F	Axial dynamic force
FMX	Maximum value of F_o.
F_o	Value of F at pile top (x=0)
$\bar{F}_o$	Average value of F_o between t=0 and t=t_o
f	Unit lateral friction (dynamic + static)
f^{est}	Unit lateral friction (static)
f^{est}_{max}	Maximum unit lateral friction (static)
J	Damping factor
J_s	Smith damping (shaft)
J_t	Smith damping (toe)
k	Spring constant
K	Elastic rebound
K_D	Elastic rebound (dynamic)
K_E	Elastic rebound (static)
K_r	Pile Stiffness (Equation 2)
$L;L_c$	Total and embedded pile length
q_s	Shaft quake
q_t	Toe quake
Q_p	Static tip load
Q_{pr}	Maximum static tip load
R,	RMX Maximum mobilized loads
R_e	Static resistance in element
R_{eT}	Total static resistance (shaft and toe)
R_d	Dynamic resistance in element
R_{dT}	Total dynamic resistance (shaft and toe)
R_d^{tip}	Mobilized dynamic resistance at the pile tip
R_m	Total resistance in element (R_m=R_e+R_d)
R_{mT}	Total resistance (R_{mT}=R_{eT}+R_{dT})
R_p	Toe resistance
$s;s_f$	Set; final set
SLT	Static Load Test
s_{to}	Set for t=to
$S;S_p$	Cross sections of pile (shaft and tip)
t;t_o	Time; Time for v=0
u	Axial displacement in element
$v;v_o$	Velocity of element; v at pile top (x=0)
x	Depth
Z	Impedance equals to $E.S/c$
W_H; W_P	Hammer and Pile Weights
α	Parameter of Velloso (Equation 3)
β	Relationship between tip and total loads
κ	Reduction parameter of Paikowsky and Chernauskas (Equation 4)
λ	Leonard and Lovell's coefficient (Equation 3)
ξ	Parameter of Uto's Formula (Equation 6)
ζ	Aoki's parameter
ρ	Specific mass of pile